Chien-Hsuan Ko[1,2]
Di Li[1]
Amirreza Malekanfard[1]
Yao-Nan Wang[3]
Lung-Ming Fu[2,4]*
Xiangchun Xuan[1]

[1]Department of Mechanical Engineering, Clemson University, Clemson, SC, USA
[2]Graduate Institute of Materials Engineering, National Pingtung University of Science and Technology, Taiwan
[3]Department of Vehicle Engineering, National Pingtung University of Science and Technology, Pingtung, Taiwan
[4]Department of Engineering Science, National Cheng Kung University, Tainan, Taiwan

Received July 23, 2018
Revised October 4, 2018
Accepted October 4, 2018

Research Article

Electroosmotic flow of non-Newtonian fluids in a constriction microchannel

Insulator-based dielectrophoresis has to date been almost entirely restricted to Newtonian fluids despite the fact that many of the chemical and biological fluids exhibit non-Newtonian characteristics. We present herein an experimental study of the fluid rheological effects on the electroosmotic flow of four types of polymer solutions, i.e., 2000 ppm xanthan gum (XG), 5% polyvinylpyrrolidone (PVP), 3000 ppm polyethylene oxide (PEO), and 200 ppm polyacrylamide (PAA) solutions, through a constriction microchannel under DC electric fields of up to 400 V/cm. We find using particle streakline imaging that the fluid elasticity does not change significantly the electroosmotic flow pattern of weakly shear-thinning PVP and PEO solutions from that of a Newtonian solution. In contrast, the fluid shear-thinning causes multiple pairs of flow circulations in the weakly elastic XG solution, leading to a central jet with a significantly enhanced speed from before to after the channel constriction. These flow vortices are, however, suppressed in the strongly viscoelastic and shear-thinning PAA solution.

Keywords:
Electrokinetic / Electroosmosis / Microfluidics / Shear thinning / Viscoelasticity
DOI 10.1002/elps.201800315

Additional supporting information may be found online in the Supporting Information section at the end of the article.

1 Introduction

Insulator-based dielectrophoresis (iDEP) is an emerging technique that has been increasingly used to manipulate a variety of particles (e.g., cells, viruses, and DNA molecules) in microfluidic devices [1–4]. It exploits the in-channel insulating structures to generate electric field gradients for particle focusing [5, 6], trapping [7–9], patterning [10], enrichment [11–13], sorting [14–17], etc. Compared to the traditional electrode-based dielectrophoresis [18, 19], iDEP microdevices are easier to fabricate, inerter to electro-chemical reactions, and less prone to fouling [1–4]. Moreover, as DC electric fields can be used either alone or along with AC electric fields to drive the particulate suspension via electroosmotic flow, pressure-driven pumping (which involves moving parts) is not needed for iDEP devices [20, 21].

Correspondence: Prof. Xiangchun Xuan, Department of Mechanical Engineering, Clemson University, Clemson, SC 29634-0921, USA.
E-mail: xcxuan@clemson.edu

Abbreviations: **AC**, alternating current; **DC**, direct current; **iDEP**, insulator-based dielectrophoresis; **PAA**, polyacrylamide; **PDMS**, polydimethylsiloxane; **PEO**, polyethylene oxide; **PVP**, polyvinylpyrrolidone; **XG**, xanthan gum

The performance of iDEP is dependent on both particle DEP and fluid electroosmosis regardless of the particle charge. The former motion is a strong function of the particle's size, shape, and electric properties (i.e., conductivity and permittivity) [22, 23]. Its velocity can be controlled by shaping the insulating structure or varying the electric field [24]. For fluid electroosmosis, iDEP devices have thus far been almost entirely restricted to work with Newtonian fluids [1–4]. The insulating structures can cause electrothermal flow [25–31] and/or induced charge electroosmotic flow [32–39] due to the amplified Joule heating in the fluid around them and their own electrical polarization, respectively [40, 41]. However, many of the chemical (e.g., colloidal suspensions and polymer solutions) and biological (e.g., blood, saliva, and DNA solutions) fluids are actually complex, exhibiting non-Newtonian characteristics [42, 43]. It is therefore important to know if and how the fluid rheological properties may affect the electroosmotic flow in iDEP devices.

As reviewed recently by Zhao and Yang [44], there have been several dozens of theoretical (and numerical) papers on electroosmotic flow and particle electrophoresis in

*Additional Corresponding Author: Prof. Lung-Ming Fu
E-mail: loudyfu@mail.ncku.edu.tw

Color online: See the article online to view Figs. 1–7 in color.

non-Newtonian fluids. Various constitutive equations [45–54] have been used to simulate the fluid rheological properties. In contrast, experimental studies in this direction have been significantly lacking. Bryce and Freeman [55] observed an unstable electroosmotic flow of polyacrylamide (PAA) solution through a constriction microchannel when the DC electric field reaches a threshold value. This extensional instability was, however, found [56] to not really enhance the electroosmotic mixing. Lu et al. [57] reported an unexpected oscillation of polystyrene microparticles that travel along with the electroosmotic flow of polyethylene oxide (PEO) solutions through a constriction microchannel. They found in a later paper [58] that particles traveling against the electroosmotic flow experience no oscillations in the constriction and can be focused toward the channel center. More recently, Pimenta and Alves [59] investigated the electroosmotic flow of PAA solutions through a cross-shaped microchannel. They observed a direct transition from a steady symmetric flow to a time-dependent asymmetric flow in both the cross-slot and flow-focusing configurations.

We perform in this work an experimental study of the sole and combined effects of fluid elasticity and shear thinning on the electroosmotic flow of four types of polymer solutions in a typical iDEP device, i.e., a constriction microchannel, via submicron particle streakline imaging. The obtained electroosmotic flow patterns are compared among the four types of buffer-based polymer solutions as well as against that of a Newtonian buffer solution. Moreover, the particle velocities before and after the constriction under varying DC electric fields are investigated.

2 Experiment

2.1 Microdevice

The iDEP microdevice was fabricated with polydimethylsiloxane (PDMS) using the standard soft lithography technique. The detailed fabrication procedure is referred to our earlier work [5]. The device contains a 40 μm-deep straight rectangular microchannel with a 2D widthwise constriction in the middle. The top- and side-walls of this channel are PDMS while the bottom wall is glass. The main channel is 400 μm wide and 1 cm long while the constriction is 40 μm wide and 200 μm long. At each end of this channel, there is a 6-mm diameter well (3-4 mm deep) that serves as the inlet or outlet reservoir for the working fluid. Freshly prepared microchannels were used in any test of a new working fluid, and were primed with pure water for 10 min to render the surface property uniform and reproducible. Figure 1 shows a top-view picture of this constriction microchannel.

2.2 Fluids

Five types of aqueous solutions were tested, among which four are non-Newtonian fluids and the fifth is a

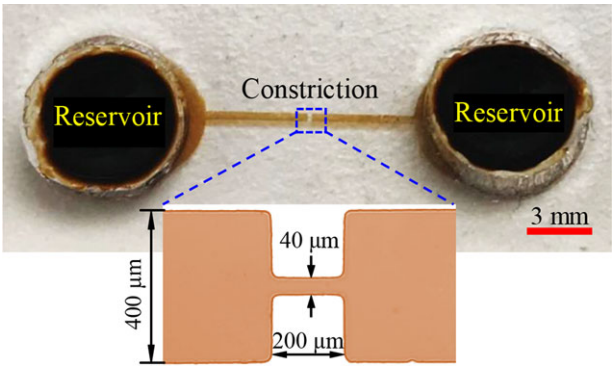

Figure 1. Top-view picture of an iDEP microdevice used in experiments. The inset shows the dimensions of the widthwise constriction in the middle of a straight rectangular microchannel.

Newtonian fluid for the control experiment. They were all prepared in 1 mM phosphate buffer (pH ≈ 7.4) with a measured electric conductivity of 200 μS/cm: (1) pure buffer solution, Newtonian fluid; (2) 2000 ppm xanthan gum (XG) solution (Tokyo Chemical Industry), weakly elastic fluid with a strong shear-thinning effect [60]; (3) 5% polyvinylpyrrolidone (PVP) solution (molecular weight, M_w = 360 kDa, Sigma–Aldrich), purely elastic fluid with a negligible shear-thinning effect [61]; (4) 3000 ppm PEO solution (M_w = 4 MDa, Sigma–Aldrich), viscoelastic fluid with a weak shear-thinning effect [62]; (5) 200 ppm PAA solution (M_w = 18 MDa, Polysciences), strongly viscoelastic and shear-thinning fluid [63]. Table 1 summarizes their rheological properties (when the phosphate buffer is absent), which are directly adapted from the literature due to the lack of measuring equipment in our lab. As the concentration of the added phosphate is low (46 ppm monosodium phosphate and 179 ppm disodium phosphate), we assume the addition of buffer does not significantly affect the fluid rheological properties.

We employ two dimensionless numbers to characterize the shear-thinning and elasticity effects of each of the prepared solutions. The former is reflected by the power-law index, n (Table 1). Note that $n = 1$ indicates a Newtonian or Boger (i.e., purely elastic [64]) fluid. The smaller value of $n < 1$, the stronger the shear thinning effect is (note: weakly shear thinning if $n \geq 0.65$ as suggested by Lindner et al. [65]). The fluid elasticity effect is characterized by the elasticity number, El, which is the ratio of the Weissenberg number, Wi, to the Reynolds number, Re [66],

$$Re = \frac{2\rho V w_c h}{\eta(w_c + h)} \tag{1}$$

$$Wi = \lambda \bar{\dot{\gamma}} = \frac{2\lambda V}{w_c} \tag{2}$$

$$El = \frac{Wi}{Re} = \frac{\lambda \eta (w_c + h)}{\rho w_c^2 h} \tag{3}$$

In the above, ρ is the fluid density, V is the average fluid velocity in the constriction, w_c is the constriction

Table 1. Rheological properties and dimensionless numbers (where the subscript EK indicates the values were estimated using the electrokinetic particle velocity at an average electric field of 250 V/cm) of the prepared solutions at 20°C. Also listed are the measured electrokinetic particle mobility, μ_{EK}, electroosmotic fluid mobility, μ_{EO}, and electrophoretic particle mobility, μ_{Ep}, in each solution. Note that the electric field direction is defined as the positive direction in the determination of mobility values

Solution	Polymer concentration	λ (ms)	η_0 (mPa•s)	n	Re_{EK}	Wi_{EK}	El	μ_{EK}	μ_{EO} ($\times 10^{-8}$ m^2/V·s)	μ_{Ep}
Buffer	0	0	1	1	0.12	0	0	–1.01	0.54	–1.55
XG[a)]	2000 ppm	~0	3680	0.34	0.006	0	~0	–1.18	0.75	–1.93
PVP[b)]	5%	2.2	28	~1	0.0043	0.33	77.0	–1.24	0.06	–1.30
PEO[c)]	3000 ppm	2.6	7.9	0.81	0.017	0.39	23.0	–1.29	0.14	–1.43
PAA[d)]	200 ppm	95	22	0.377	0.032	14.25	449.4	–1.15	1.82	–2.97

a) Japper-Jaafar et al. [60]; b) Liu et al. [61]; c) De Santo et al. [62]; d) Poole and Escudier [63].

Table 2. Parameters involved in the Carreau–Yasuda model for estimating the viscosity of the prepared XG, PEO, and PAA solutions (without the phosphate salt, estimated at 20°C)

Solution	Time constant, λ_{CY}	Fitting parameter, a	Infinite shear viscosity, η_∞
XG[a)]	21.5 s	0.81	2.24 mPa•s
PEO[b)]	6.3 ms	1.15	0[c)]
PAA[d)]	0.551 s	0.623	2.62 mPa•s

a) Japper-Jaafar et al. [60]; b) De Santo et al. [62]; c) Not the real value of η_∞ for the PEO solution, extracted from the formula (S1) in the Supplemental Material of De Santo et al. [62]; d) Poole and Escudier [63].

width, h is the microchannel height, η is the fluid viscosity evaluated at the average shear-rate inside the constriction, $\overline{\dot{\gamma}} = 2V/w_c$, and λ is the fluid relaxation time. Note that a larger value of $El > 1$ indicates a stronger elasticity effect.

For the pure buffer and PVP solutions with a negligible shear-thinning effect, η is equal to the zero-shear-rate fluid viscosity, $\eta = \eta_0$ (Table 1). For the shear thinning XG, PEO, and PAA solutions, η is shear-rate dependent and estimated using the Carreau–Yasuda model [67] at the average fluid shear rate in the channel constriction, $\overline{\dot{\gamma}}$,

$$\frac{\eta - \eta_\infty}{\eta_0 - \eta_\infty} = \left[1 + \left(\lambda_{CY}\overline{\dot{\gamma}}\right)^a\right]^{(n-1)/a} \quad (4)$$

where η_∞ is the infinite-shear-rate viscosity, λ_{CY} is a time constant, and a is a fitting parameter (see their values in Table 2). The estimated values of Re, Wi, and El at an average electrokinetic particle velocity in the constriction of the microchannel, $V = 3$ mm/s (or equivalently 0.3 mm/s in the main channel), are presented in Table 1. This reference velocity was estimated using the measured particle speed at an average electric field of 250 V/cm over the channel length, which is a typical value in all our tests except the PAA solution. We note that the electroosmotic flow of non-Newtonian fluids is essentially inertialess because $Re < 0.1$.

2.3 Method

Fluorescent polystyrene spheres of 0.5 μm diameter (Bangs Laboratories) were used as tracers (10^7-10^8 particles per mL) to visualize the flow pattern of the prepared non-Newtonian and Newtonian fluids. A high-voltage DC power supply (Glassman High Voltage Inc.) was used to generate the electroosmotic flow through platinum electrodes that were inserted into the liquid of the end-channel reservoirs. The average electric field magnitude (equal to the imposed voltage drop divided by the overall 1 cm channel length) was kept no more than 400 V/cm (note the electric field at the constriction is roughly ten times this value) to minimize the effect of Joule heating [68]. The motion of tracing particles was recorded through an inverted fluorescent microscope (Nikon Eclipse TE2000U, Nikon Instruments) equipped with a CCD camera (Nikon DS-Qi1Mc). The captured images were processed using the Nikon imaging software (NIS-Elements AR 2.30).

Particles were observed to move against the electric field direction in all tests. Their velocities before and after the channel constriction (at least a few channel widths away from the constriction) were obtained using the particle tracking velocimetry (i.e., particle velocity is equal to the particle's travelling distance divided by the time span of measurement) for only those particles that were traveling along the channel centerline. It is important to note that the observed electrokinetic motion of particles is a superposition of fluid electroosmosis and particle electrophoresis. We assume particle electrophoresis follows the electric field line, which, according to Zhao and Yang [44], is reasonable for thin electric double layers (10 nm thick in 1 mM buffer) and small particles that are not too close to any boundaries. The electrokinetic mobility, μ_{EK}, was determined from the slope of the linear trendline of the experimentally determined particle velocities vs. electric field. As the average electric field was used in this analysis, the obtained electrokinetic mobility values are only approximations to the real values. The electroosmotic velocity in each prepared solution was measured by tracking the front of neutral Rhodamine B dyes (Sigma–Aldrich, 50 μM) with time. This velocity divided by the average electric field gives the electroosmotic mobility, μ_{EO}. The electrophoretic

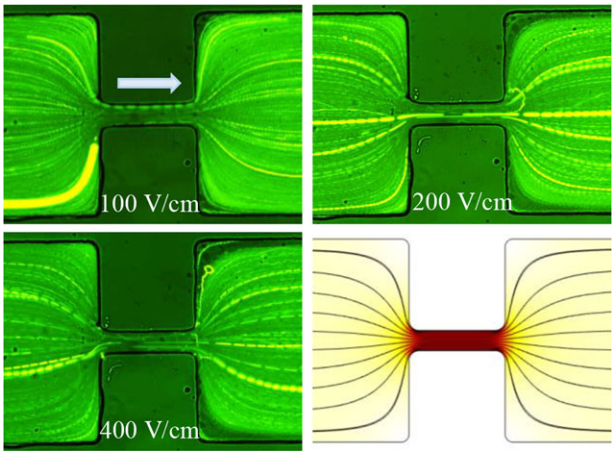

Figure 2. Electroosmotic flow of Newtonian buffer solution through a constriction microchannel. The upper-row and lower-left panels show the streak images of tracing particles under the DC electric fields of 100, 200, and 400 V/cm, respectively. The lower-right panel shows the numerically predicted electric field lines (similar to fluid streamlines) and contour (the darker color, the larger magnitude). The block arrow indicates the moving direction of tracing particles, which is against the electric field direction.

particle mobility, μ_{EP}, was then estimated from $\mu_{EK} - \mu_{EO}$. These obtained mobility values in each solution are presented in Table 1.

3 Results and discussion

3.1 Newtonian buffer solution

Figure 2 shows the top-view images of tracing particles in the electroosmotic flow of Newtonian buffer solution ($n = 1$ and $El = 0$) through the constriction of the microchannel. Nearly symmetric streaklines are observed before and after the constriction when the DC electric field is varied from 100 V/cm to 400 V/cm. They are consistent with the numerically predicted electric field lines (obtained from a 2D COMSOL® model, see the Supporting Information for the modeling detail) in Fig. 2, which are similar to the fluid streamlines in a purely electroosmotic flow [26]. This phenomenon indicates that the lateral migration of the tracing particles due to DEP or inertial lift is insignificant because of the small particle size and small particle Reynolds number [69]. The average electrokinetic particle velocity along the channel centerline remains unvaried before and after the channel constriction, and increases linearly with the applied electric field (see Supporting Information Fig. S2). The obtained electrokinetic particle mobility is about 1.0×10^{-8} m^2/(V·s).

3.2 Weakly elastic shear-thinning XG solution

Figure 3 shows the images of tracing particles in the electroosmotic flow of 2000 ppm pseudoplastic XG solution ($n = 0.34$ and $El \sim 0$) through the constriction microchannel. Under an electric field of 100 V/cm, we observe three pairs of counter-rotating fluid circulations that are highlighted by the arrowed loops in Fig. 3 (left panel). The two pairs after the constriction both appear near the corners (the onset of the larger pair of vortices is at the electric field of around 25 V/cm while the onset of the smaller pair is at 65 V/cm) and are adjacent to each other with opposing rotating directions. In contrast, the pair of fluid circulations before the constriction first appears near the lips of the constriction (at the electric field of nearly 100 V/cm) and then extends toward the corners with increasing electric field. Their sizes and strengths both grow as the electric field increases from 100 V/cm to 400 V/cm. Meanwhile, the formation of these fluid circulations is accompanied by a fluid jet (more precisely, a jet of particles) along the channel centerline. Moreover, due to the conservation of mass, the fluid jet has different velocities before and after the constriction as a result of the size and strength differences in the fluid circulations therein. This can be viewed from the distinct opening angles of the fluid jet, α and β, before and after the channel constriction as highlighted on the image in Fig. 3 (upper-right panel).

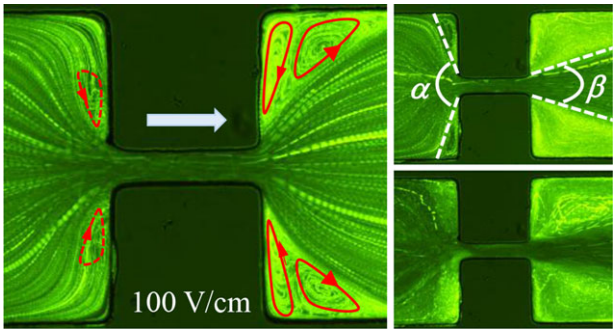

Figure 3. Electroosmotic flow of 2000 ppm XG solution through the channel constriction. The left panel shows the zoom-in view of the streak image of tracing particles under a 100 V/cm DC electric field, where the block arrow indicates the overall particle moving direction through the channel and the arrowed loops highlight the local fluid circulations. The upper-right and lower-right panels show the particle images under the electric fields of 200 and 400 V/cm, respectively, where the highlighted angles, α and β, on the upper-right image measure the opening angles of the fluid jet before and after the channel constriction, respectively.

Figure 4A compares the measured electrokinetic velocities of tracing particles along the channel centerline before and after the constriction. Both velocities increase with increasing electric field, whose relationships can each be fitted well to a positive-power trendline. It is important to note that we select the power-law fit because it represents the simplest and best fitting to the experimental data points. The rationale behind such a selection is currently unverified though it should be associated with the fluid shear thinning effect. We will perform in our future work a comprehensive experimental and numerical study of the parametric effects on electroosmotic flow of XG solutions in constriction microchannels. As viewed from the equations of the trendlines in Fig. 4A, the

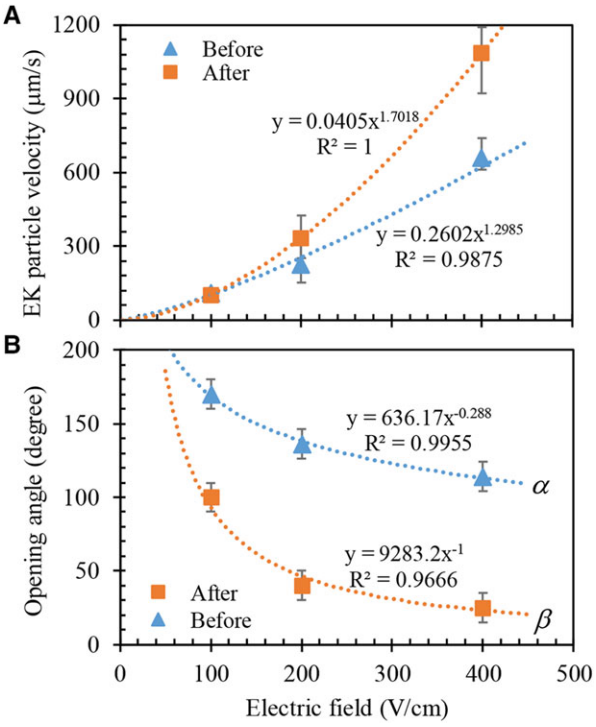

Figure 4. Electric field effect on the velocity of tracing particles (only those along the centerline of the channel were tracked) (A), and the opening angles (see the highlighted angles, α and β, on the image in Fig. 3) of the fluid jet (B) in the electroosmotic flow of 2000 ppm XG solution before and after the channel constriction. All symbols (with error bars) represent the experimental data measured from the images in Fig. 3. The dotted lines represent the power trendlines (both the equation and the R^2 value of each trendline are displayed on the charts) that are best fitted to the experimental data points.

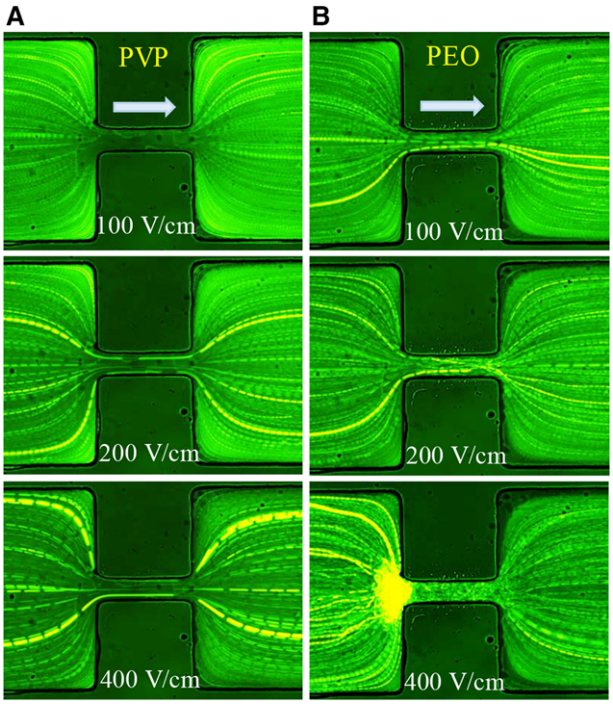

Figure 5. Top-view streak images of tracing particles in the electroosmotic flow of 5% PVP (A) and 3000 ppm PEO (B) solutions through the channel constriction under varying DC electric fields. The bright zone at the mouth of the constriction on the bottom-right image is a result of the locally enriched tracing particles. The block arrows indicate the moving direction of tracing particles.

particle velocity after the constriction has a higher power index, leading to an increasingly large gap from that before the constriction as the electric field increases. Such variations are consistent with those in the opening angles of the fluid jet before and after the constriction in Fig. 4B. Specifically, each opening angle decreases with the increase of electric field in the form of a negative-power trendline, leading to an enhanced fluid velocity in the form of a positive-power trendline (Fig. 4A). Moreover, the opening angle after the constriction is not only smaller but also decreases more quickly than that before the constriction, which explains why the fluid velocity after the constriction becomes increasingly larger under a higher electric field in Fig. 4A. The mechanism behind the formation of fluid circulations and central fluid jet is currently unclear, which is believed to be associated with the strong shear-thinning effect of the XG solution.

3.3 Viscoelastic PVP and PEO solutions with negligible or weak shear-thinning effects

As viewed from the listed values of the power index, n, and elasticity number, El, in Table 1, 5% PVP and 3000 ppm PEO solutions exhibit comparable elasticity (especially, their Weissenberg numbers are nearly identical and of the order of 1) and shear-thinning ($n > 0.8$) effects. Therefore, their electroosmotic flow patterns in the constriction microchannel are expected to be similar as demonstrated by the streaking images in Fig. 5. Interestingly, these images are not visually different from those in the Newtonian buffer solution under varying DC electric fields in Fig. 2. Such a similarity may suggest that the fluid elasticity effect alone does not strongly affect the electroosmotic flow pattern. The measured electrokinetic mobility of tracing particles is around 1.25×10^{-8} m^2/(V·m) in both the PVP and PEO solutions (see Supporting Information Figs. S3 and S4), which is 25% more than that in the pure buffer solution. This is surprising considering the fact that the viscosities of the two viscoelastic solutions are both significantly larger than that of the buffer solution (Table 1). One potential reason is the polymer-induced variation of zeta potential [70], and another is the formation of near-wall polymer-depleted skimming layer [71].

However, there is one exception in the PEO solution, where the tracing particles are seen to accumulate at the mouth of the channel constriction under the electric field of 400 V/cm (and higher) in Fig. 5. This phenomenon was not observed in any other prepared solutions in our experiments. We also tested the electroosmotic flow of 1000 ppm PEO solution (data not shown), which is less viscous and less shear

thinning than 3000 ppm, under the identical experimental conditions. Accumulation of tracing particles was still observed when the applied DC electric field was increased to 600 V/cm (and higher). We therefore tend to think that there might be a formation of some sort of gels inside the channel constriction under large electric fields, which significantly slows down the entering particles (the measured electrokinetic mobility drops by half compared to the two lower electric fields in Fig. 5) for a dielectrophoretic trapping. It is noted that a buildup of crystallized PEO strands has been reported to occur at the reentrant corner of a contraction channel in a pressure-driven flow with a moderate Reynolds number [72]. We are unsure if there are any similarities between these two observations.

3.4 Strongly viscoelastic and shear-thinning PAA solution

Figure 6 shows the streakline images of tracing particles in the electroosmotic flow of 200 ppm PAA solution ($n = 0.377$ and $El \gg 1$) through the channel constriction. Under a DC electric field of 200 V/cm (note this value was found to vary between experiments, although the overall trend remains similar to Fig. 6) or higher, we observed the formation of a large gel before the constriction that captured most of the particles (lower-right image in Fig. 6). However, the few particles that escaped from the gel could still pass through the constriction. The formation of such gelled rafts in PAA solution under high electric fields has also been reported previously [54, 58]. Under the electric fields of less than 200 V/cm, the tracing particles before the constriction appear to move a little slower than after it. Similar to the observation in the XG solution in Fig. 3, this phenomenon seems to be also associated with the formation of a central fluid jet after the constriction as highlighted by the angle, β, in Fig. 6 (lower-left image). However, the fluid jet before the channel constriction is not obvious and no fluid circulations occur anywhere, which are different from the observations in the nearly equally shear-thinning XG solution in Fig. 3.

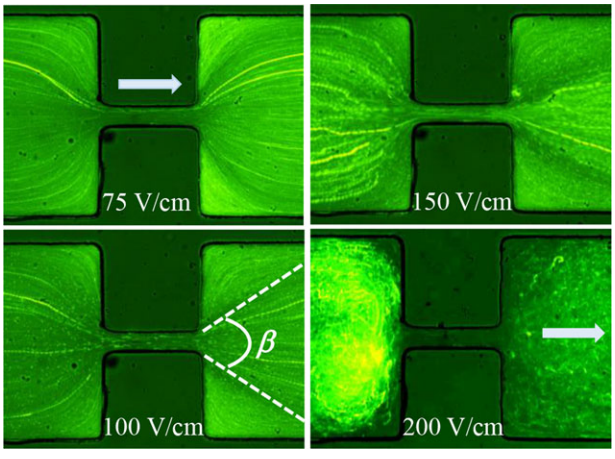

Figure 6. Top-view streak images of tracing particles in the electroosmotic flow of 200 ppm PAA solution through the channel constriction under varying DC electric fields. The highlighted angle, β, on the lower-left image measures the opening angle of the central fluid jet after the channel constriction. The majority of the particles are captured by a large gel formed before the constriction under the electric field of 200 V/cm. The block arrow indicates the particle moving direction.

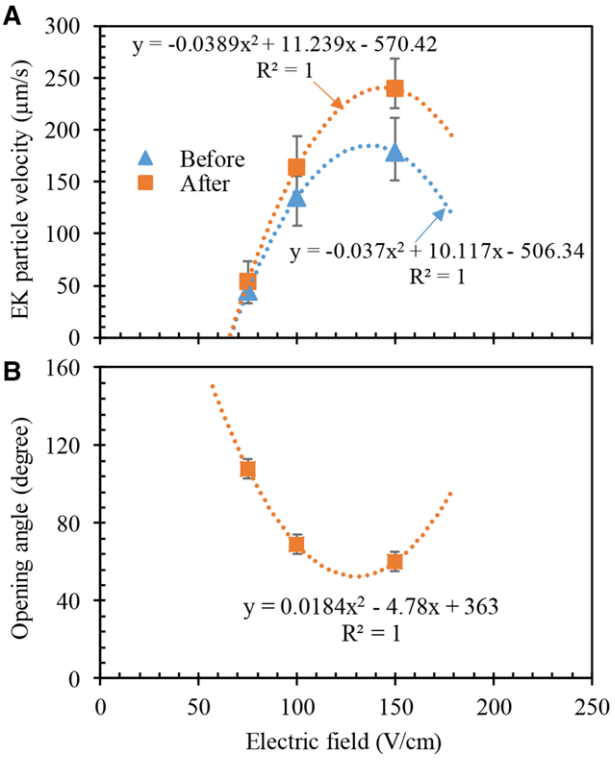

Figure 7. Electric field effect on the measured velocity of tracing particles (only those along the centerline of the channel were tracked) (A), and the measured opening angle (see the highlighted angle, β, on the image in Fig. 6) of the fluid jet (B) in the electroosmotic flow of 200 ppm PAA solution through the channel constriction. All symbols (with error bars) represent the experimental data measured from the images in Fig. 6. The dotted lines represent the quadratic polynomial trendlines (both the equation and the R^2 value of each trendline are displayed on the charts) that are best fitted to the experimental data points.

Figure 7A compares the measured electrokinetic particle velocities along the centerline before and after the constriction of the microchannel. Both velocities first increase (≤150 V/cm) and then decrease (up to 200 V/cm) when the DC electric field is increased. However, the particle velocity after the constriction has a larger magnitude than before the constriction, for which each trend can be fitted well to a negative quadratic (i.e., second order) polynomial function (see the trendlines on the chart, where the data points at 200 V/cm are excluded). This phenomenon is related to the variation of the opening angle, β, of the fluid jet after the channel constriction, which is well fitted to a positive quadratic trendline in Fig. 7B. We again note that the quadratic fit represents the simplest and best fitting to the experimental data points.

The rationale for this selection is still unknown, although it is definitely related to the strong shear thinning and elasticity effects of the PAA solution.

4 Concluding remarks

We have conducted a comprehensive experimental study of fluid rheological effects on the electroosmotic flow of five types of aqueous solutions through a constriction microchannel. It is found that the weakly shear-thinning, viscoelastic PVP and PEO solutions exhibit a very similar electroosmotic flow pattern to the Newtonian buffer solution. This similarity may indicate that the fluid elasticity alone has an insignificant impact on the steady-state electroosmotic flow pattern. In contrast, the fluid shear-thinning effect alone is found to cause three pairs of counter-rotating fluid circulations in the weakly elastic XG solution near the entry and exit corners of the channel constriction. These vortices further lead to the formation of a central fluid jet whose velocity is significantly increased from before to after the constriction and correlated well with the opening angle due to the conservation of mass. Such electric field-dependent phenomena are not observed in the strongly viscoelastic and shear-thinning PAA solution. It is important to note that the polymer chemistry, which is not discussed in the current work, may also play a role in the electroosmotic flow of non-Newtonian fluids [44]. We hope this work will stimulate more experimental and theoretical studies in the future.

This work was supported in part by NSF under Grant No. CBET-1704379 (X.X.).

The authors have declared no conflict of interest.

5 References

[1] Srivastava, S. K., Gencoglu, A., Minerick, A. R., *Anal. Bioanal. Chem.* 2010, *399*, 301–321.

[2] Regtmeier, J., Eichhorn, R., Viefhues, M., Bogunovic, L., Anselmetti, D., *Electrophoresis* 2011, *32*, 2253–2273.

[3] Li, M., Li, W., Zhang, J., Alici, G., Wen, W., *J. Phys. D: Appl. Phys.* 2014, *47*, 063001.

[4] Jubery, T. Z., Srivastava, S. K., Dutta, P., *Electrophoresis* 2014, *35*, 691–713.

[5] Zhu, J., Xuan, X., *Electrophoresis* 2009, *30*, 2668–2675.

[6] Church, C., Zhu, J., Wang, G., Tzeng, T. J., Xuan, X., *Biomicrofluidics* 2009, *3*, 044109.

[7] Chou, C. F., Tegenfeldt, J. O., Bakajin, O., Chan, S. S., Cox, E. C., Darnton, N., Duke, T., Austin, R. H,, *Biophys. J.* 2002, *83*, 2170–2179.

[8] Braff, W. A., Pignier, A., Buie, C. R., *Lab Chip* 2012, *12*, 1327–1331.

[9] Nakano, A., Camacho-Alanis, F., Ros, A., *Analyst* 2015, *140*, 860–868.

[10] Kale, A., Lu, X., Patel, S., Xuan, X., *J. Micromech. Microeng.* 2014, *24*, 075007.

[11] Barrett, L. M., Skulan, A. J., Singh, A. K., Cummings, E. B., Fiechtner, G. J., *Anal. Chem.* 2005, *77*, 6798–6804.

[12] Lapizco-Encinas, B. H., Davalos, R. V., Simmons, B. A., Cummings, E. B., Fintschenko, Y., *J. Microbiol. Methods* 2005, *62*, 317–326.

[13] Lewpiriyawong, N., Yang, C., Lam, Y. C., *Microfluid. Nanofluid.* 2012, *12*, 723–733.

[14] Lapizco-Encinas, B. H., Simmons, B. A., Cummings, E. B., Fintschenko, Y., *Electrophoresis* 2004, *25*, 1695–1704.

[15] Pysher, M. D., Hayes, M. A., *Anal. Chem.* 2007, *79*, 4552–4557.

[16] Hawkins, B. G., Smith, A. E., Syed, Y. A., Kirby, B. J., *Anal. Chem.* 2007, *79*, 7291–7300.

[17] Kang, Y. J., Li, D. Q., Kalams, S. A., Eid, J. E., *Biomed. Microdev.* 2008, *10*, 243–249.

[18] Gascoyne, P. R. C., Vykoukal, J., *Electrophoresis* 2002, *23*, 1973–1983.

[19] Hughes, M. P., *Electrophoresis* 2002, *23*, 2569–2582.

[20] Gagnon, Z. R., *Electrophoresis* 2011, *32*, 2466–2487.

[21] Cetin, B., Li, D., *Electrophoresis* 2011, *32*, 2410–2427.

[22] Pohl, H. A., *Dielectrophoresis*, Cambridge University Press, Cambridge, 1978.

[23] Pethig, R., *Biomicrofluidics* 2010, *4*, 022811.

[24] Jesu´s-Pe´rez, N. M., Lapizco-Encinas, B. H., *Electrophoresis* 2011, *32*, 2331–2357.

[25] Hawkins, B. J., Kirby, B. J., *Electrophoresis* 2010, *31*, 3622–3633.

[26] Sridharan, S., Zhu, J., Hu, G., Xuan, X., *Electrophoresis* 2011, *32*, 2274–2281.

[27] Kale, A., Patel, S., Hu, G., Xuan, X., *Electrophoresis* 2013, *34*, 674–683.

[28] Kumar, A., Williams, S.J., Chuang, H.S., Green, N.G., Wereley, S.T., *Lab Chip* 2011, *11*, 2135–2148.

[29] Gallo-Villanueva, R., Sano, M., Lapizco-Encinas, B., Davalos, R., *Electrophoresis* 2014, *35*, 352–361.

[30] Prabhakaran, R. A., Zhou, Y., Patel, S., Kale, A., Song, Y., Hu, G., Xuan, X., *Electrophoresis* 2017, *38*, 572–579.

[31] Kale, A., Song, L., Lu, X., Yu, L., Hu, G., Xuan, X., *Electrophoresis* 2018, *39*, 887–896.

[32] S. K. Thamida, H. C. Chang, *Phys. Fluid.* 2002, *14*, 4315.

[33] Eckstein, Y., Yossifon, G., Seifert, A., Miloh, T., *J. Colloid Interface Sci.* 2009, *338*, 243–249.

[34] Yossifon, G., Frankel, I., Miloh, T., *Phys. Fluid.* 2006, *18*, 117108.

[35] Zehavi, M., Yossifon, G., *Phys. Fluid.* 2014, *26*, 082002.

[36] Harrison, H., Lu, X., Patel, S., Thomas, C., Todd, A., Johnson, M., Raval, Y., Tzeng, T., Song, Y., Wang, J., Li, D., Xuan, X, *Analyst* 2015, *140*, 2869–2875.

[37] Zehavi, M., Boymelgreen, A., Yossifon, G., *Phys. Rev. Appl.* 2016, *5*, 044013.

[38] Prabhakaran, R. A., Zhou, Y., Zhao, C., Hu, G., Song, Y., Wang, J., Yang, C., Xuan, X., *Phys. Fluid.* 2017, *29*, 062001.

[39] Ren, Y., Liu, W., Tao, Y., Hui, M., Wu, Q., *Micromachines* 2018, *9*, 102.

[40] Cetin, B., Li, D., *Electrophoresis* 2008, *29*, 994–1005.

[41] Wang, Q., Dingari, N. N., Buie, C. R., *Electrophoresis* 2017, *38*, 2576–2586.

[42] D'Avino, G., Greco, F., Maffettone, P. L., *Annu. Rev. Fluid Mech.* 2017, *49*, 341–360.

[43] Lu, X., Liu, C., Hu, G., Xuan, X., *J. Colloid Interface Sci.* 2017, *500*, 182–201.

[44] Zhao, C., Yang, C., *Adv. Colloid. Interf. Sci.* 2013, *201–202*, 94–108.

[45] Olivares, M. L., Vera-Candioti, L., Berli, C. L. A., *Electrophoresis* 2009, *30*, 921–929.

[46] Zhao, C., Yang, C., *Electrophoresis* 2013, *34*, 662–667.

[47] Afonso, A. M., Alves, M.A., Pinho, F.T., *J. Non-Newton. Fluid Mech.* 2009, *159*, 50–63.

[48] Zhao, C., Yang, C., *Appl. Math. Comput.* 2011, *211*, 502–509.

[49] Sousa, J. J., Afonso, A. M., Pinho, F. T., Alves, M. A., *Microfluid. Nanofluid.* 2011, *10*, 107–122.

[50] Afonso, A. M., Pinho, F.T., Alves, M. A., *J. Non-Newton. Fluid Mech.* 2012, *179–180*, 55–68.

[51] Yeh, L. H., Hsu, J. P., *Microfluid. Nanofluid.* 2009, *7*, 383–392.

[52] Zhao, C., Yang, C., *Biomicrofluidics* 2011, *5*, 014110.

[53] Khair, A. S., Posluszny, D. E., Walker, L. M., *Phys. Rev. E* 2012, *85*, 016320.

[54] Bandopadhyay, A., Chakraborty, S., *Phys. Rev. E* 2012, *85*, 056302.

[55] Bryce, R. M., Freeman, M. R., *Phys. Rev. E* 2010, *81*, 036328.

[56] Bryce, R. M., Freeman, M. R., *Lab Chip* 2010, *10*, 1436–1441.

[57] Lu, X., Patel, S., Zhang, M., Joo, S., Qian, S., Ogale, A., Xuan, X., *Biomicrofluid.* 2014, *8*, 021802.

[58] Lu, X., DuBose, J., Qian, S., Joo, S., Xuan, X., *Biomicrofluid.* 2015, *9*, 014108.

[59] Pimenta, F., Alves, M. A., *J. Non-Newton. Fluid Mech.* 2018, *259*, 61–77.

[60] Japper-Jaafar, A., Escudier, M. P., Poole, R. J., *J. Non-Newton. Fluid Mech.* 2010, *165*, 1357–1372.

[61] Liu, C., Xue, C., Chen, X., Shan, L., Tian, Y., Hu, G., *Anal. Chem.* 2015, *87*, 6041–6048.

[62] De Santo, I., D'Avino, G., Romeo, G., Greco, F., Maffettone, P. L., *Phys. Rev. Appl.* 2014, *2*, 064001.

[63] Poole, R. J., Escudier, M. P., *J. Non-Newton. Fluid Mech.* 2004, *117*, 25–46.

[64] James, D. F., *Annu. Rev. Fluid Mech.* 2009, *41*, 129–142.

[65] Lindner, A., Bonn, D., Meunier, J., *Phys. Fluids* 2000, *12*, 256–261.

[66] Rodd, L. E., Scott, T. P., Boger, D. V., Cooper-White, J. J., McKinley, G. H., *J. Non-Newton. Fluid Mech.* 2005, *129*, 1–22.

[67] Yasuda, K., Armstrong, R. C., Cohen, R. E., *Rheo. Acta* 1981, *20*, 163–178.

[68] Xuan, X., *Electrophoresis* 2008, *29*, 33–43.

[69] Zhang, J., Yan, S., Yuan, D., Alici, G., Nguyen, N. T., Warkiani, M. E., Li, W., *Lab Chip* 2016, *16*, 10–34.

[70] Wong, I., Ho, C. M., *Microfluid. Nanofluid.* 2009, *7*, 291–306.

[71] Sadek, S. H., Pimenta, F., Pinho, F. T., Alves, M. A., *Electrophoresis* 2017, *38*, 1022–1037.

[72] James, D. F., Saringer, J. H., *J. Non-Newton. Fluid Mech.* 1982, *11*, 317–339.

